

“© 2020 IEEE. Personal use of this material is permitted. Permission from IEEE must be obtained for all other uses, in any current or future media, including reprinting/republishing this material for advertising or promotional purposes, creating new collective works, for resale or redistribution to servers or lists, or reuse of any copyrighted component of this work in other works.”

E. Alonso et al., "A Machine Learning Framework for Pulse Detection During Out-of-Hospital Cardiac Arrest" in IEEE Access, vol. 8, pp. 161031-161041, 2020, doi:
[10.1109/ACCESS.2020.3021310](https://doi.org/10.1109/ACCESS.2020.3021310).

Date of publication xxxx 00, 0000, date of current version xxxx 00, 0000.

Digital Object Identifier 10.1109/ACCESS.2017.DOI

A Machine Learning Framework for Pulse Detection During Out-of-hospital Cardiac Arrest

ERIK ALONSO¹, UNAI IRUSTA², (Member, IEEE), ELISABETE ARAMENDI², (Member, IEEE) and MOHAMUD R. DAYA.³

¹Department of Applied Mathematics, University of the Basque Country UPV/EHU, 48013 Bilbao, Spain

²Department of Communications Engineering, University of the Basque Country UPV/EHU, 48013 Bilbao, Spain

³Department of Emergency Medicine, Oregon Health & Science University (OHSU), Portland, OR 97239 USA

Corresponding author: Erik Alonso (e-mail: erik.alonso@ehu.eus).

This work was supported partially by the Spanish Ministry of Science, Innovation and Universities through Grant RTI2018-101475-BI00, jointly with the Fondo Europeo de Desarrollo Regional (FEDER), and in part by the Basque Government through Grant IT-1229-19.

ABSTRACT The availability of an automatic pulse detection during out-of-hospital cardiac arrest (OHCA) would allow the rapid identification of cardiac arrest and the prompt detection of return of spontaneous circulation. The aim of this study was to develop a reliable pulse detection algorithm using the electrocardiogram (ECG) and thoracic impedance (TI), the signals available in most defibrillators. The dataset used in the study consisted of 1140 ECG and TI segments from 187 OHCA patients, whereof 792 were labelled as pulse generating rhythm (PR) and 348 as pulseless electrical activity (PEA) by a pool of experts in OHCA. First, an adaptive filtering scheme was used to extract the impedance circulation component and its first derivative from the TI. Then, the wavelet decomposition of the ECG was carried out to obtain the different subband components and the denoised ECG. Pulse/no-pulse (PR/PEA) discrimination features were extracted from those signals and fed into a support vector machine (SVM) classifier that made the pulse/no-pulse decision. A quasi-stratified and patient wise nested cross validation procedure was used to select the best feature subset and to tune the SVM hyperparameters. This procedure was repeated 50 times to estimate the statistical distributions of the performance metrics of the method. The optimal solution consisted in a five feature classifier that yielded a mean (standard deviation) sensitivity, specificity, balanced accuracy and total accuracy of 92.4% (0.7), 93.0% (0.8), 92.7% (0.5) and 92.6% (0.5), respectively. When compared to available methods, our solution presented an improvement in balanced accuracy of at least 2.5 points. A reliable pulse detection algorithm for OHCA using the signals available in defibrillators was accomplished.

INDEX TERMS Machine learning, adaptive filtering, stationary wavelet transform (SWT), support vector machine (SVM), out-of-hospital cardiac arrest (OHCA), thoracic impedance, electrocardiogram (ECG), pulse detection.

I. INTRODUCTION

EVERY year out-of-hospital cardiac arrest (OHCA) accounts for about 300 000 deaths among adults in the United States [1]. The majority of OHCAs occur at home and are unwitnessed [2], [3]. The survival rate is around 10% in witnessed OHCA treated by emergency medical services (EMS) [4]. An early recognition of cardiac arrest is determinant for the patient's survival as it leads (1) to a rapid dispatch of the EMS, (2) to an immediate initiation of bystander cardiopulmonary resuscitation (CPR) which has been

reported to double or quadruple survival [5]–[9], and (3) to an early defibrillation that has been associated with increased survival [10]. The essential electrophysiological equipment used for treatment and monitoring in OHCA is the defibrillator, either a monitor/defibrillator used by trained EMS personnel or automated external defibrillators (AEDs) prepared to be used by untrained lay rescuers.

Recognizing cardiac arrest can be challenging. Confirming the absence of circulation through a carotid pulse check has been found inaccurate for both lay rescuers and healthcare

personnel [11], [12]. Assessment of 'normal breathing' proposed in current resuscitation guidelines [13] as an indicator of circulation has been proved unreliable [14], [15]. Pulse checks and breathing assessments are time consuming and introduce unnecessary CPR interruptions, needing in average 9.5 s for carotid pulse checks [11] and 12 s for breathing assessments [14]. These interruptions in CPR compromise coronary perfusion pressure and are detrimental for the survival of the patient [16]. Therefore, there is a need for reliable pulse detectors that might be incorporated into defibrillators. Such methods would allow for an early and rapid identification of the cardiac arrest, and would shorten CPR interruptions to confirm absence of circulation. In addition, they would allow for a rapid detection of the return of spontaneous circulation (ROSC), which would result in a prompt initiation of post-resuscitation care and avoidance of potentially harmful chest compressions or administration of adrenaline in spontaneously beating hearts.

Several solutions based on the digital processing of biomedical signals have been proposed to detect pulse during cardiac arrest. Doppler-ultrasound in the carotid [17] and nasal photoplethysmography [18], [19] have been used to detect pulse in swine models of cardiac arrest. Recent studies used the regional cerebral oxygen saturation measured through near-infrared spectroscopy to predict ROSC during in- and out-of-hospital cardiac arrest [20], [21]. Acceleration signals measured on the common carotid artery from in-hospital cardiac arrest patients [22] or acquired from accelerometer-based CPR feedback devices in a porcine model of cardiac arrest [23] have also been used to develop pulse detectors. An abrupt rise of end tidal CO₂ (EtCO₂) has recently been reported as a specific but non-sensitive predictor of ROSC in OHCA [24], [25]. Several studies have used the ECG [26]–[28] or thoracic impedance (TI) [29], [30] to detect pulse. Others however have combined ECG and TI [31]–[33], ECG and EtCO₂ [34] or ECG, TI and EtCO₂ [35].

Most current commercial defibrillators record the ECG and TI signals through the defibrillation pads. The ECG is used to analyze the underlying cardiac rhythm and to decide whether defibrillation is necessary. The TI signal is used to check the correct skin-pad contact and to adjust defibrillation energy. Therefore, a pulse detector based on both signals might be incorporated into defibrillators without hardware modifications and could be used by both lay rescuers (AEDs) and healthcare professionals (monitor/defibrillators).

Pulse detection in cardiac arrest is typically framed as the discrimination between pulseless electrical activity (PEA) and pulse-generating rhythm (PR) [26], [29], [31]–[33]. Both PEA and PR present a (quasi)-normal ECG with visible QRS complexes, the electrical activity associated with the depolarization of the ventricles in a heartbeat. However, during PEA the heart loses its contractile function so there is a dissociation between the electrical and mechanical activities of the heart, and thus no blood flow [36]. In contrast, PR presents a normal electrical and mechanical activity, and thus effective blood flow. Differences between PR and PEA are

not always perceptible in the ECG, but PR usually presents regular and narrow complexes, while PEA might show more irregular and wider QRS complexes [36]. In the TI small fluctuations ($<100\text{ m}\Omega$) correlated with the QRS complexes can be observed for PR, but not for PEA [37], [38].

This study presents a new method for pulse detection during OHCA using the ECG and TI signals. The approach uses an adaptive filter to extract the circulatory-related component from the TI, from here on referred to as impedance circulation component (ICC), and a support vector machine (SVM) classifier based on features extracted from the ECG and ICC to discriminate PEA and PR. The manuscript is organized as follows: Section II provides a description of the study dataset; Section III details the feature engineering methods including the extraction of the ICC, and the process of extracting features from the ECG, TI and ICC; the architecture used for feature selection, and the optimization and evaluation of the method are described in Section IV; results and discussion are described in Section V; and finally conclusions are presented in Section VI.

II. DATA MATERIALS

The study cohort was composed of 187 OHCA patients treated by the Tualatin Valley Fire & Rescue (Tigard, OR, USA) using the Philips HeartStart MRx (Philips Healthcare, MA, USA) monitor/defibrillator between 2010 and 2014. Each episode contained ECG, TI and capnography signals. The amplitude resolution per least significant bit and the sampling frequency of the ECG and TI signals were 1.03 mV and 250 Hz, and 0.74 mΩ and 200 Hz, respectively. All signals were converted to a Matlab (Matick, MA, USA) format and the TI was resampled to match the ECG sampling rate. The powerline interferences and spiky noise in the ECG were removed by using a 60 Hz notch filter and a Hampel filter, respectively. Other sources of noise were removed through wavelet denoising techniques, as described in Section III.

The episodes were visually reviewed to extract those segments that during resuscitation were used to analyze the patient's heart rhythm. Only segments with visible QRS complexes (PEA or PR) and a minimum duration of 5 s were included in the dataset. Those segments were then annotated as PEA or PR by three expert reviewers: an emergency medicine doctor, a cardiologist and a biomedical engineer. To make a decision the reviewers were provided with annotations of ROSC made in the field. Abrupt increases and decreases (from below 20 to above 35 mmHg and viceversa) indicated ROSC and loss of ROSC, respectively. Resuming chest compressions after an interval to analyze the heart rhythm was also considered as an indicator of no ROSC. Annotation discrepancies among reviewers were further reviewed until a consensus PEA/PR annotation was reached.

The dataset used in the study consisted of a total of 1140 segments, 792 PR and 348 PEA, containing the ECG and TI signals. The mean (standard deviation, SD) duration of the segments was 8.2(1.7) s, 8.0(1.7) s for PR and 8.5(1.7) s for PEA segments.

III. FEATURE ENGINEERING

The starting point for feature extraction were the ECG signal, $s_{\text{ecg}}(n)$, and TI signal, $s_{\text{imp}}(n)$, where the sample index n is related to time by $t = n/f_s$, with a sampling frequency of $f_s = 250 \text{ Hz}$. The feature extraction process was composed of three phases. First, an adaptive filter was used to extract the ICC, $s_{\text{icc}}(n)$, from $s_{\text{imp}}(n)$. Then, the wavelet decomposition of the ECG signal was carried out to obtain the different subband components and the denoised signal, $s_{\text{den}}(n)$. Finally, features were computed from $s_{\text{icc}}(n)$, its first derivative $s_{\text{dicc}}(n)$, the subband components and $s_{\text{den}}(n)$. Fig. 1 shows examples of the most relevant signals and subbands used for feature extraction for a PEA and a PR segment.

A. ADAPTIVE EXTRACTION OF THE ICC

In patients presenting pulse the $s_{\text{imp}}(n)$ can be expressed using the following additive model [31], [32]:

$$s_{\text{imp}}(n) = s_{\text{rest}}(n) + s_{\text{icc}}(n) \quad (1)$$

where $s_{\text{rest}}(n)$ contains the impedance's baseline value and artifacts mainly due to pads movement and skin-pad con-

tact. The ejection of blood into the aorta caused by each effective contraction of the heart produces fluctuations in the impedance, that is the $s_{\text{icc}}(n)$ component. Consecutive fluctuations slightly vary on amplitude and duration. Therefore, the nature of $s_{\text{icc}}(n)$ is quasi-periodic and can be modeled using a Fourier series with N terms of slowly time varying amplitudes and frequencies:

$$s_{\text{icc}}(n) = \sum_{k=1}^N a_k(n) \cos(k \omega_0(n) n) + b_k(n) \sin(k \omega_0(n) n) \quad (2)$$

where N represents the number of harmonics. The Fourier coefficients $a_k(n)$ and $b_k(n)$ represent the in-phase and quadrature amplitudes of the model, and $\omega_0(n) = 2\pi f_0(n)/f_s$ its fundamental frequency. The Hamilton-Tompkins algorithm [39], [40] was used to detect the sample indices of the R peaks of the QRS complexes (r_i), but some adaptations were made for OHCA data such as shortening the refractory period and lowering the threshold coefficient [26]. The sample indices r_i were used to compute $f_0(n)$ as follows:

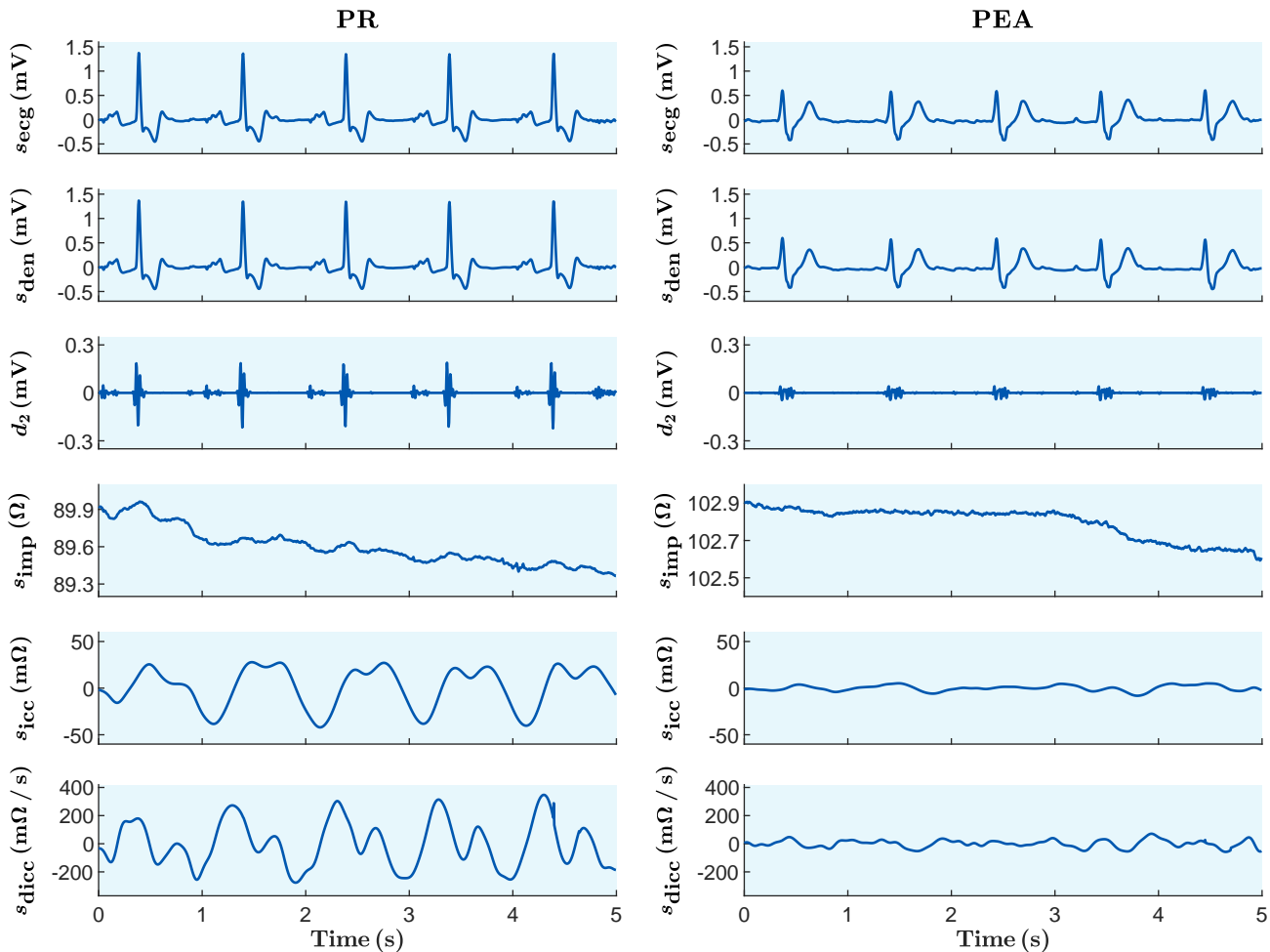


FIGURE 1. Wavelet analysis of the ECG signal and adaptive extraction of the ICC for a PR (left) and PEA (right) segments. From top to bottom, the original ECG signal (s_{ecg}), the denoised ECG (s_{den}), a relevant subband of the ECG (d_2), the original TI signal (s_{imp}), the ICC (s_{icc}) and its first derivative (s_{dicc}).

$$f_0(n) = \frac{f_s}{r_{i+1} - r_i} \quad \forall n \in (r_i, r_{i+1}] \quad (3)$$

There is therefore a variation in $f_0(n)$ for consecutive QRS intervals, but it remains constant within each interval. For estimating $a_k(n)$ and $b_k(n)$, three different adaptive algorithms were inspected: Recursive Least Squares (RLS) [31], [41], [42], Least Mean Square (LMS) [41], [43] and Kalman filtering [44], [45]. For each algorithm two were the parameters to be tuned: N and $\mu/\lambda/q$, the constants that regulate the stability and convergence rate of the LMS/RLS/Kalman algorithms, respectively. Larger values of μ (step size) or q (variance of the process noise) and smaller values of λ (forgetting factor) result in a faster rate of convergence but could turn the process unstable [41]–[45].

B. STATIONARY WAVELET TRANSFORM

The multiresolution analysis of the ECG signal, $s_{\text{ecg}}(n)$, was carried out using the stationary wavelet transform (SWT). Basically, the SWT consists in the application, at each level of decomposition, of a pair of conjugate quadrature low-pass, $h_{j-1}(n)$, and high-pass, $g_{j-1}(n)$, filters to produce at the next level two new sequences, the approximation (a_j) and detail (d_j) coefficients, as follows:

$$a_j(n) = h_{j-1}(n) * a_{j-1}(n) \quad (4)$$

$$d_j(n) = g_{j-1}(n) * a_{j-1}(n) \quad (5)$$

where $(*)$ denotes convolution, $a_0(n) = s_{\text{ecg}}(n)$ and the high-pass filters at each level are obtained by time reversal and a π radian frequency shift of the low-pass filters as:

$$g_j(n) = (-1)^{n+1} h_j(M-1-n) \quad (6)$$

where M is the length of the filter. The SWT, unlike the discrete wavelet transform, does not decimate a_j and d_j at each level and therefore, they always have the same length as the original signal a_0 . Instead, filters at each level are upsampled by a factor of 2 with respect to filters at previous level. Thus, $h_j(n)$ is obtained by inserting a zero between each adjacent pair of samples of $h_{j-1}(n)$.

After some preliminary tests (see details in the supplementary materials), a Coiflet 3 mother wavelet was used to decompose $s_{\text{ecg}}(n)$ into $J = 8$ decomposition levels which generated detail coefficients $d_1 - d_8$ and approximation coefficient a_8 . Detail coefficients $d_2 - d_8$ were soft denoised using the universal threshold described in [46] and used to synthesize the denoised ECG signal, s_{den} , by recursively evaluating

$$a_{j-1}(n) = \frac{1}{2}(g'_j(n) * a_j(n) + h'_j(n) * d_j(n)) \quad (7)$$

from $j = J, \dots, 1$, where $g'_j(n) = g_j(M-1-n)$ and $h'_j(n) = h_j(M-1-n)$ are the time-reversed versions of the decomposition filters, known as synthesis filters. The synthesized $a_0(n)$ coefficient corresponded to s_{den} which only retained frequency components in the $0.5 - 62.5$ Hz band. Although most commercial defibrillators only analyze

the ECG in the $0.5 - 30$ Hz frequency band to recommend defibrillation, for pulse detection we decided to retain d_2 ($31.25 - 62.5$ Hz subband). These components are important to discriminate PEA from PR because electrical conduction is better in PR than in PEA resulting in narrower QRS complexes that produce higher spectral components [47].

C. FEATURE EXTRACTION

A total of 40 PEA/PR discrimination features were computed from s_{icc} , s_{dicc} , s_{den} and the denoised detail coefficients $d_2 - d_8$.

The first 8 features were the mean peak-to-trough amplitude (MPT), the SD of the peak-to-trough amplitude (SDPT), mean area (MA) [43] and fuzzy entropy (FuzzyEn) [48]–[50] of s_{icc} and s_{dicc} . The following 21 features were the energy (Enrg) [41], Kurtosis (Kurt) [51] and FuzzyEn of the detail coefficients $d_2 - d_8$. The next 9 features were computed from s_{den} including the number of QRS complexes (nQRS), mean (MRR) and SD (SDRR) of the interval between R waves [31], [32], mean (MPP) and SD (SDPP) of the QRS complex amplitude [31], median QRS width (QRSw) [32], amplitude spectrum area (AMSA) [52], energy at high frequency bands (Sxx) [26], [53] and FuzzyEn. Finally, 2 additional features were computed, the mean cross power [33] between s_{icc} and s_{den} (CP), and between s_{icc} and detail coefficient d_7 (CPd7). A detailed description of the features can be obtained in the references provided above, and a Matlab implementation of these features in <https://github.com/erik-alonso/PEA-PR-features>.

IV. ARCHITECTURE OF THE MODEL AND EVALUATION

A nested cross-validation (CV) architecture was used to train the model and evaluate its performance [54]. The inner loop consisted in a 5-fold CV scheme for feature selection using a wrapping approach, while in the outer loop 10-fold CV was used to optimize the classifiers' parameters and evaluate the performance of the model. In both inner and outer loops random quasi-stratified patient-wise partitions of the data were used. Partitions maintained at least 90% of the PEA and PR proportions of the original dataset. The model was evaluated in terms of sensitivity (SE, capacity to correctly detect PR), specificity (SP, capacity to correctly detect PEA), accuracy (ACC, correct classification ratio), and balanced accuracy (BAC, mean of SE and SP). The performance metrics were calculated always in the test folds by comparing the model's PR/PEA decisions with the ground truth labels set by expert reviewers. The PEA and PR class imbalance was addressed by weighting each class according to their proportion of samples.

The nested CV procedure was repeated 50 times using different random partitions to estimate the statistical distributions of the performance metrics. All the results are given as mean (SD) of the values obtained in the 50 repetitions of the experiments.

A. FEATURE SELECTION

Feature selection was carried out in the inner loop using the sequential floating forward selection (SFFS) algorithm [55], and a multivariate logistic regression algorithm to evaluate the classification performance of the feature subsets. The SFFS consists in applying first sequential forward selection to add a new feature and then a number of backward steps (*backtracking*) as long as the resulting feature subsets perform better than the ones selected before at those levels [56]. Therefore, features added in previous steps might be removed in posterior steps. This procedure avoids the nesting effect of purely sequential selection algorithms [57], namely sequential forward selection (SFS) and sequential backward selection (SBS).

The SFFS algorithm was run until the best V -feature subset was selected, using the maximization of the BAC as feature inclusion/exclusion criterion.

B. CLASSIFICATION ALGORITHM

The classification algorithm was based on a support vector machine (SVM) classifier [58], [59], which is an extension of the maximal margin hyperplane to accomodate non-linear decision boundaries between classes.

Given training instance-label pairs (\mathbf{x}_i, y_i) for $i = 1, \dots, l$ where $\mathbf{x}_i \in \mathbb{R}^V$ is a vector containing the z -scores of the V features selected in the inner CV loop and $y_i \in \{-1, 1\}$ denotes the ground truth for PEA (no pulse) and PR (pulse), respectively; the SVM requires to solve the following optimization problem:

$$\begin{aligned} \min_{w_0, w} \quad & \frac{1}{2} \|\mathbf{w}\|^2 + C \sum_{i=1}^l \epsilon_i \\ \text{subject to} \quad & y_i(\mathbf{w}^T \phi(\mathbf{x}_i) + w_0) \geq 1 - \epsilon_i, \\ & \epsilon_i \geq 0 \quad \forall i. \end{aligned} \quad (8)$$

where w_0 and \mathbf{w} are the coefficients of the maximal margin hyperplane, C is a nonnegative tuning parameter, ϵ_i are variables that indicate if the i^{th} training instance is in the incorrect side of the margin or the hyperplane, and ϕ is the basis function that maps training instances, \mathbf{x}_i , into a higher dimensional space.

Given the solutions w_0 and \mathbf{w} of (8), the SVM decision function, can be expressed as

$$G(\mathbf{x}) = \text{sign}(\mathbf{w}^T \phi(\mathbf{x}) + w_0) \quad (9)$$

with a test instance, \mathbf{x} , classified as PEA/PR for negative/positive signs, respectively. However, in practice there is no need to specify the transformation $\phi(\mathbf{x})$ and only knowledge of the kernel function is required

$$K(\mathbf{x}, \mathbf{x}_i) = \langle \phi(\mathbf{x}), \phi(\mathbf{x}_i) \rangle \quad (10)$$

to calculate inner products in the higher dimentional space. Thus, the SVM decision function can also be written as

$$\begin{aligned} G(\mathbf{x}) &= \text{sign}(\mathbf{w}^T \phi(\mathbf{x}) + w_0) \\ &= \sum_{i=1}^l \alpha_i y_i K(\mathbf{x}, \mathbf{x}_i) + w_0 \end{aligned} \quad (11)$$

with nonzero coefficients α_i only for the support vectors, i.e those training instances i for which the constraints in (8) are exactly met. In this study a radial basis kernel function was used:

$$K(\mathbf{x}, \mathbf{x}_i) = \exp(-\gamma \|\mathbf{x} - \mathbf{x}_i\|^2). \quad (12)$$

Therefore, the hyperparameter optimization of the classifier consists in tuning C and γ . The cost parameter C regulates the bias-variance trade-off of the SVM and γ defines the adaptability of the decision boundary [54], [60]. Hyperparameters C and γ were tuned in the outer loop through a 30×30 grid search in the ranges $1 \leq C \leq 100$ and $0.03 \leq \gamma \leq 1.26$ to maximize the BAC of the SVM classifier. The development and optimization of the SVM classifier was carried out using the LIBSVM library [61].

V. RESULTS AND DISCUSSION

The main results from the experiments and their contextualization are presented in this section. First, the search for the optimal working points of the adaptive filters for the extraction of the ICC is conducted. Second, the importance of feature selection is analyzed by ranking the selected features and by evaluating the effect on performance of different feature selection algorithms and the number of features, V , included in the model. Then, the effect of the duration of the signal segment, L , on the performance of the model is analyzed. Finally, a comparative assessment with the most relevant available solutions based on ECG and TI signals is presented.

A. CONFIGURATION OF THE ADAPTIVE FILTERS

Fig. 2 represents the mean BAC obtained by the model in the 50 repetitions of the nested CV procedure for different configurations of the adaptive filters. The results are shown as a function of the number of harmonics in the model N , and the tuning parameter governing tracking (λ , μ or q) for the RLS, LMS and Kalman filters. In this analysis, the pulse detection algorithm was based on $V = 5$ features extracted from segments with a duration of $L = 5$ s. All configurations showed a mean BAC above 90%, and the maximum BAC was obtained with a small number of harmonics, $N = 2$ for the RLS and $N = 3$ for the LMS and Kalman filters. Overall, adding more harmonics ($N \geq 4$) resulted in a decrease in the BAC. This is well aligned with the results in [31] where the RLS filter with $N = 3$ was used to obtain the ICC. In our study, the RLS and LMS filters outperformed the Kalman filter, both reaching a mean BAC above 92%. The RLS is more complex and computationally demanding than the LMS, but converges faster than the LMS. In a setting

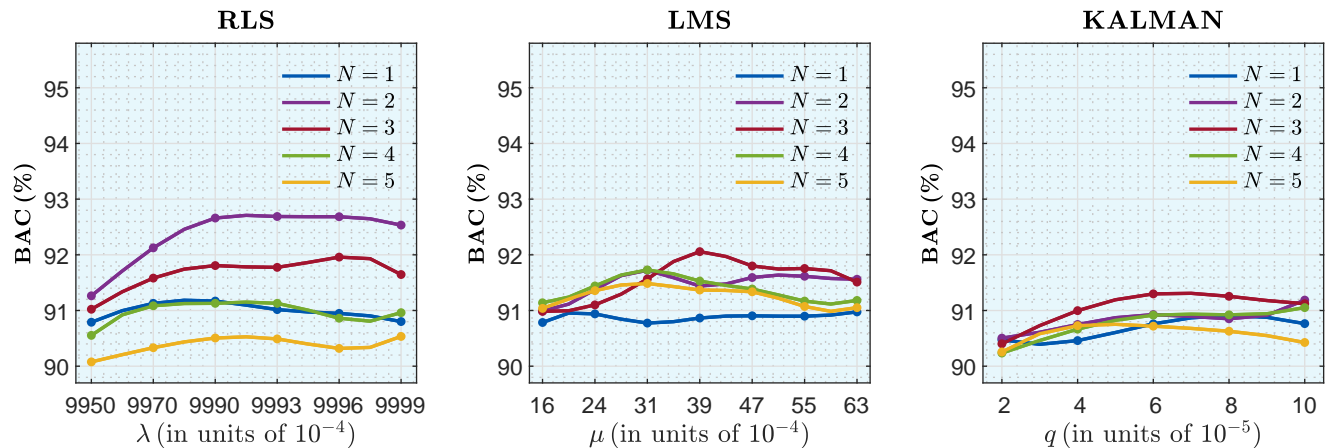


FIGURE 2. Mean BAC of the pulse detection algorithm in the 50 repetitions of the nested CV procedure when RLS/LMS/Kalman adaptive filters are used to extract the ICC. The BAC is depicted for different values of the parameter governing tracking (λ , μ or q) and the complexity of the model determined by the number of harmonics, N .

with short signal segments this can be advantageous, in our analysis for $L = 5$ s the best BAC was 0.6 points larger for the RLS than for the LMS. Table 1 shows in greater detail the performance of the pulse detection algorithm with respect to N for the optimal values of the tuning parameters $\lambda = 0.9993$, $\mu = 39 \cdot 10^{-4}$ and $q = 6 \cdot 10^{-5}$ for RLS, LMS and Kalman filters, respectively.

From here on, the rest of the analyses were carried out using the RLS filter with $\lambda = 0.9993$ and $N = 2$.

B. ON THE IMPORTANCE OF FEATURE SELECTION

Fig. 3 shows the mean BAC as a function of the number of features used in the model. This analysis was carried out using $L = 5$ s segments and the SFFS feature selection algorithm. The results were compared to 3 other feature selection algorithms: SFS, SBS and Plus- l take-away- r [57], more concretely PTA(3,2) in our analysis. The trends were similar independently of the feature selection algorithm. Adding features increased the mean BAC until performance plateaued when 4-6 features were included in the model. Including more than 6 features resulted in a decreased BAC. The pulse detection algorithm presenting the maximum BAC (92.7%) was based on $V = 5$ features selected through the SFFS algorithm, although it was only 0.1 points higher than when PTA(3,2) was used. The SFFS algorithm differs from

the PTA(l, r) algorithm [57] in that (1) it allows a dynamic and self-controlled backtrack without the need of predicting the best fixed values for (l, r) ; and (2) it also allows for more than one sweep through feature subsets [55]. The nesting effect negatively affected the mean BAC obtained via the SFS and SBS algorithms, with a decrease between 0.3–0.8 points with respect to that obtained by SFFS and PTA(3,2) in the high performance plateau (4-6 features).

Features were ranked in Table 2 according to P_{TS} , the proportion of times they were selected in the inner loop of the 50 repetitions of the nested CV procedure (50 repetitions \times 10-fold CV = 500 feature selection loops). The SFFS algorithm and $V = 5$ features were considered to compute the ranking. Table 2 also shows the mean area under the curve (AUC) obtained from the receiver operating characteristic curve analysis carried out on the test folds. The top in the ranking included features extracted from ECG and TI signals in (1) time domain (MA, SDPT, MRR) [43], (2) frequency domain (Enrg) [41], (3) the complexity analysis (FuzzyEn) [48] and the statistical distribution of the samples (Kurt) [51]. The feature ranking showed the importance of retaining detail coefficient d_2 as its FuzzyEn and Enrg turned out to be the second and sixth most selected features with a mean AUC of 0.93 and 0.91, respectively. Overall, most of the features presented a high discriminative power with up to 11 features

TABLE 1. Performance metrics of the pulse detection algorithm for optimal values $\lambda/\mu/q$ of the adaptive filters and different number of harmonics, N .

N	RLS ($\lambda = 0.9993$)				LMS ($\mu = 39 \cdot 10^{-4}$)				KALMAN ($q = 6 \cdot 10^{-5}$)			
	SE (%)	SP (%)	BAC (%)	ACC (%)	SE (%)	SP (%)	BAC (%)	ACC (%)	SE (%)	SP (%)	BAC (%)	ACC (%)
1	90.5 (0.9)	91.5 (1.0)	91.0 (0.6)	90.8 (0.7)	90.9 (1.0)	90.9 (1.0)	90.9 (0.7)	90.9 (0.8)	90.8 (1.2)	90.7 (1.1)	90.8 (0.8)	90.8 (0.9)
2	92.4 (0.7)	93.0 (0.8)	92.7 (0.5)	92.6 (0.5)	91.2 (1.2)	91.6 (0.9)	91.4 (0.7)	91.4 (0.8)	91.4 (1.4)	90.4 (0.9)	90.9 (0.9)	91.1 (1.0)
3	91.2 (1.0)	92.4 (1.0)	91.8 (0.7)	91.5 (0.8)	92.0 (1.1)	92.1 (1.1)	92.1 (0.8)	92.0 (0.8)	91.7 (1.0)	90.9 (1.1)	91.3 (0.7)	91.5 (0.8)
4	90.6 (1.3)	91.7 (1.1)	91.1 (0.8)	90.9 (0.9)	91.5 (1.1)	91.6 (0.8)	91.5 (0.8)	91.5 (0.9)	91.3 (1.2)	90.5 (1.0)	90.9 (0.8)	91.1 (0.9)
5	89.7 (1.4)	91.3 (1.0)	90.5 (0.8)	90.2 (1.0)	91.4 (1.2)	91.4 (0.9)	91.4 (0.8)	91.4 (0.9)	91.0 (1.2)	90.4 (1.0)	90.7 (0.8)	90.8 (0.9)

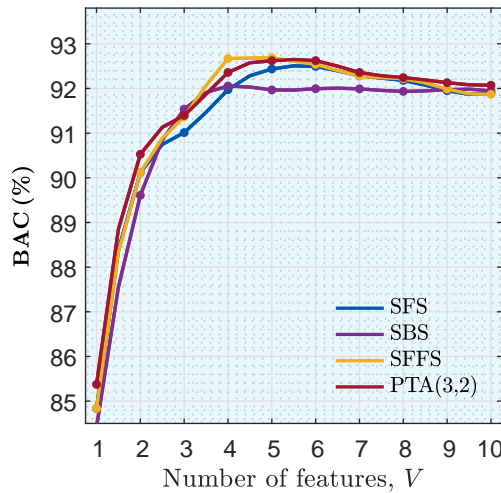


FIGURE 3. Mean BAC of the pulse detection algorithm in the 50 repetitions of the nested CV procedure when different algorithms are used to select a varying number of features, V .

TABLE 2. Features ranked by the P_{TS} in the 50 repetitions of the nested CV procedure and their discriminative power in terms of AUC.

Feature	P_{TS}	AUC	Feature	P_{TS}	AUC
MA, s_{dice}	90.6	0.93	MA, s_{icc}	3.4	0.86
FuzzyEn, d_2	77.4	0.93	FuzzyEn, d_4	3.4	0.92
SDPT, s_{icc}	72.6	0.70	FuzzyEn, d_6	2.8	0.80
FuzzyEn, s_{icc}	54.6	0.88	Enrg, d_5	2.2	0.76
SDPT, s_{dice}	40.4	0.78	CPd7	2.2	0.82
Enrg, d_2	18.4	0.91	Kurt, d_4	2.0	0.84
FuzzyEn, s_{dice}	16.8	0.86	CP	1.8	0.90
Kurt, d_7	14.8	0.75	SDRR	1.6	0.53
MRR	12.8	0.89	Enrg, d_7	1.6	0.57
FuzzyEn, d_3	12.8	0.93	Enrg, d_4	1.4	0.87
MPT, s_{dice}	8.0	0.93	MPP	1.2	0.71
Enrg, d_8	7.2	0.61	FuzzyEn, s_{den}	1.2	0.89
Kurt, d_8	7.2	0.70	FuzzyEn, d_5	1.2	0.91
nQRS	6.4	0.90	FuzzyEn, d_7	1.2	0.63
Sxx	6.0	0.91	Enrg, d_3	1.2	0.91
Kurt, d_6	6.0	0.84	Kurt, d_2	1.2	0.76
MPT, s_{icc}	4.4	0.88	Kurt, d_3	1.2	0.78
FuzzyEn, d_8	4.0	0.61	QRSw	0.6	0.68
SDPP	3.6	0.56	Enrg, d_6	0.6	0.65
Kurt, d_5	3.6	0.86	AMSA	0.4	0.89

extracted from both ECG and TI showing AUC values above 0.90. Some of the features presented a very large AUC but were not frequently selected because of the strong correlation with the top ranking features. This is particularly evident for features derived from the detail coefficients. For instance, the mean Pearson correlation coefficient between FuzzyEn for d_2 and d_4 in the test folds was 0.72 (0.02), both had AUCs above 0.91, but FuzzyEn was selected 77.4% of the times for d_2 and only 3.4% of the times for d_4 .

C. EFFECT OF SEGMENT DURATION ON PERFORMANCE

Fig. 4 shows the mean values of the performance metrics as a function of the duration of the signal segment, L . In this analysis an algorithm based on $V = 5$ features was used. Increasing L resulted in an improved BAC. However, the magnitude of those increases was smaller for $L \geq 5$ s, the mean BAC increased in over 3 points from $L = 3$ s to $L = 5$ s, but only in less than 0.3 points from $L = 5$ s to $L = 7$ s. Mean values of BAC above 90% were obtained for all segment durations except for $L = 3$ s. The SP decreased faster than the SE as segment duration decreased. An accurate identification of PEA is more challenging for shorter segment durations because of the slower and more irregular heart rates in PEA compared with PR. Moreover, at least 2 heartbeats are needed to obtain an estimate of the ICC and to derive robust classification features from the ICC and ECG. These considerations explain why increasing L from 3 s to 4 s increases the SP by over 3 points, but the SE only in 1 point.

The pulse detection algorithm presented an SE, SP, BAC and ACC above 92.4%, 93.0%, 92.7% and 92.6%, respectively, for $L \geq 5$ s. Therefore, an accurate pulse detection is possible with such segment durations. Current commercial defibrillators require on average segment durations greater than 5.2 s for an ECG rhythm analysis to reliably decide whether or not to defibrillate a patient [62]. The pulse detection algorithm could run in those intervals, and prompt the pulse/no-pulse results for the cases in which a nonshockable rhythm with QRS complexes has been identified [31], [43]. This would avoid prolonged pauses in CPR for pulse checks, which ultimately may contribute to improve survival rates.

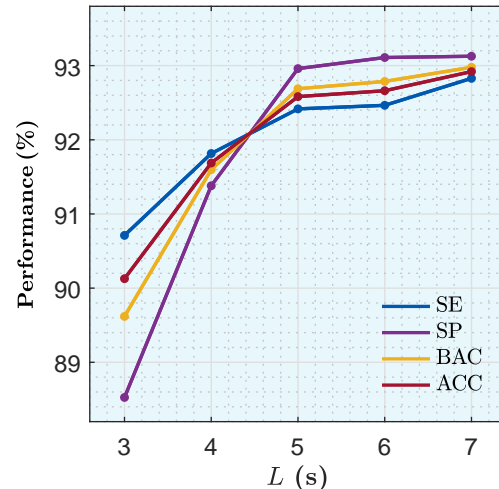


FIGURE 4. Mean values of the performance metrics (SE, SP, BAC and ACC) of the pulse detection algorithm as a function of the segment duration, L .

D. COMPARISON WITH PREVIOUS ALGORITHMS

Table 3 shows the comparison between the performance metrics for our method and three relevant methods proposed in the literature for pulse detection during OHCA using the ECG and TI. Our method (SVM) is compared to a feedforward neural network (FNN) proposed by Risdal et al. [32], a logistic regression (LR) classifier proposed by Alonso et al. [31], and a simple decision tree (SDT) recently proposed by Ruiz et al. [33]. For a fair comparison every method was replicated according to authors' descriptions in the original papers and trained/tested in the outer loop of the same 50 repetitions of the nested CV procedure used in this study. The performance metrics were obtained for a segment duration of $L = 5$ s. Our solution was based on $V = 5$ features while the rest of the methods used the optimal feature subset reported by their authors in the original manuscripts, that is 12 features in FNN, 6 features in LR and 2 features in SDT. Our method had a significantly higher ($p < 0.05$ in the McNemar test) ACC and BAC than any other method, with a minimum increase of 2.5 points in BAC and 1.6 points in ACC with respect to the best performing previous algorithms. These are large increases in performance because the BACs and ACCs of previous algorithms were already above 90%. Thus, a 1.6 point increase in ACC, from 91.0% to 92.6%, means that around 20% of the classification errors of the other classifiers are now corrected, and a 4 point increase in SP means that 40% of the PEAs incorrectly classified by other methods are correctly classified by our solution. Two are the main reasons for these advances. First, the extraction of a very good estimate of the ICC as a consequence of

TABLE 3. Performance metrics of the most relevant machine learning based pulse detection algorithms in the literature. The p -value for the McNemar test to compare the ACC and BAC of our method (SVM) to the rest of the methods is reported. All comparisons yielded a significantly higher BAC and ACC for our method.

Method	SE (%)	SP (%)	BAC (%)	ACC (%)	p -value
SVM	92.4 (0.7)	93.0 (0.8)	92.7 (0.5)	92.6 (0.5)	
FNN [32]	91.4 (1.6)	88.9 (1.7)	90.1 (0.5)	90.6 (0.7)	<0.01
LR [31]	92.3 (0.4)	88.2 (0.5)	90.2 (0.3)	91.0 (0.3)	<0.05
SDT [33]	91.8 (0.1)	76.4 (0.3)	84.1 (0.1)	87.1 (0.1)	<0.001

the extensive search for the optimum number of harmonics to model the ICC and for the best adaptive filter and the optimum value of its tuning parameter. This maximized the discriminative ability of the features extracted from the ICC estimate, with features like the MA of \hat{s}_{dicc} with an AUC of 0.93 (see Table 2). Second, the multiresolution analysis of the ECG through the SWT which allowed a rich feature extraction in the relevant ECG subbands, including the higher subband in the 31.25 – 62.25 Hz range represented by d_2 . Features extracted from d_2 showed great discriminative power with AUC values up to 0.93.

Fig. 5 shows two examples of segments misclassified by our solution, a PR (left panel) and a PEA (right panel). Each panel shows, from top to bottom, the denoised ECG (\hat{s}_{den}), detail coefficient d_2 , the ICC (s_{icc}) and its first derivative (\hat{s}_{dicc}). The misclassified PR shows narrow and regular QRS complexes with a heart rate around 100 bpm that can be

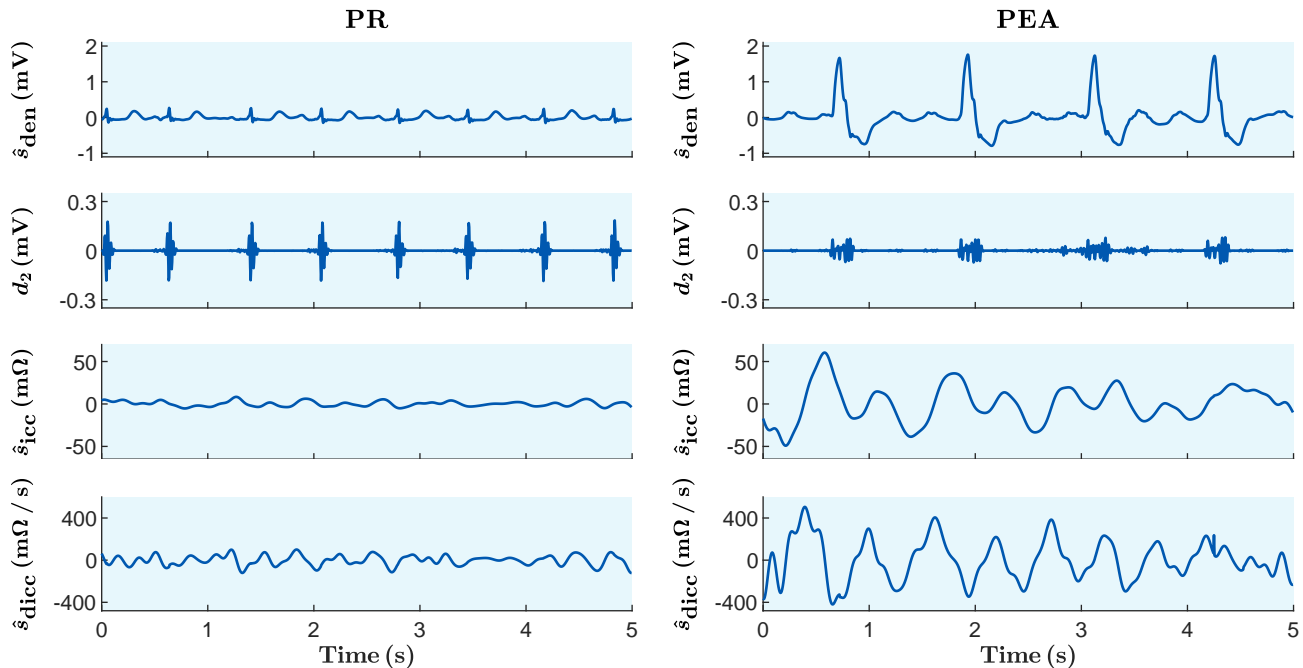


FIGURE 5. Misclassified PR (left) and PEA (right) segments. From top to bottom, the denoised ECG (\hat{s}_{den}), detail coefficient d_2 , the ICC (s_{icc}) and its first derivative (\hat{s}_{dicc}).

observed in s_{den} . This is also reflected in d_2 in the form of a considerable energy in the 31.25 – 62.25 Hz subband. Although the ECG analysis may indicate the presence of a PR, the amplitude of the ICC is small with no activity correlated with the heartbeats, which ultimately led the SVM classifier to make a no-pulse decision. On the other hand, in the misclassified PEA the denoised ECG presents wide QRS complexes with a heart rate around 50 bpm, and d_2 shows low energy which might be an indicator of PEA. Nevertheless, the highly correlated and large amplitude ICC forced the classifier to make a pulse diagnosis.

VI. CONCLUSIONS

This study presented a machine learning framework to detect pulse during OHCA. A novel feature extraction approach using the combined information in the ECG and TI was introduced, which when combined with a systematic use of machine learning techniques led to a significant increase in performance when compared to previous methods. Our method improved the BAC of the best previous methods by over 2.5 points. This algorithm could be incorporated without hardware modifications to any current defibrillator because it uses only the signals recorded through the defibrillation pads. The algorithm might also contribute to shorten or even eliminate pauses in CPR for pulse detection, which would help improve therapy and may contribute to increase survival rates.

REFERENCES

- [1] A. S. Go et al., “Heart disease and stroke statistics—2013 update: a report from the American Heart Association,” *Circulation*, vol. 127, no. 1, pp. e6–e245, Jan. 2013.
- [2] S. M. J. M. Straus et al., “The incidence of sudden cardiac death in the general population,” *Journal of Clinical Epidemiology*, vol. 57, no. 1, pp. 98–102, Jan. 2004.
- [3] J. J. de Vreeide-Swagemakers et al., “Out-of-hospital cardiac arrest in the 1990’s: a population-based study in the Maastricht area on incidence, characteristics and survival,” *Journal of the American College of Cardiology*, vol. 30, no. 6, pp. 1500–1505, Nov. 1997.
- [4] M. R. Daya et al., “Out-of-hospital cardiac arrest survival improving over time: Results from the Resuscitation Outcomes Consortium (ROC),” *Resuscitation*, vol. 91, pp. 108–115, Jun. 2015.
- [5] R. A. Waalewijn, J. G. P. Tijssen, and R. W. Koster, “Bystander initiated actions in out-of-hospital cardiopulmonary resuscitation: results from the Amsterdam Resuscitation Study (ARRESUST),” *Resuscitation*, vol. 50, no. 3, pp. 273–279, Sep. 2001.
- [6] M. Holmberg, S. Holmberg, and J. Herlitz for the Swedish Cardiac Arrest Registry, “Factors modifying the effect of bystander cardiopulmonary resuscitation on survival in out-of-hospital cardiac arrest patients in Sweden,” *European Heart Journal*, vol. 22, no. 6, pp. 511–519, Mar. 2001.
- [7] M. Holmberg et al., “Survival after cardiac arrest outside hospital in Sweden,” *Resuscitation*, vol. 36, no. 1, pp. 29–36, Jan. 1998.
- [8] M. Wissenberg et al., “Association of National Initiatives to Improve Cardiac Arrest Management With Rates of Bystander Intervention and Patient Survival After Out-of-Hospital Cardiac Arrest,” *JAMA*, vol. 310, no. 13, pp. 1377–1384, Oct. 2013.
- [9] I. Hasselqvist-Ax, J. Herlitz, and L. Svensson, “Early CPR in Out-of-Hospital Cardiac Arrest,” *The New England Journal of Medicine*, vol. 373, no. 16, pp. 1573–1574, 2015.
- [10] M. T. Blom et al., “Improved survival after out-of-hospital cardiac arrest and use of automated external defibrillators,” *Circulation*, vol. 130, no. 21, pp. 1868–1875, Nov. 2014.
- [11] J. Bahr et al., “Skills of lay people in checking the carotid pulse,” *Resuscitation*, vol. 35, no. 1, pp. 23–26, Aug. 1997.
- [12] J. Tibballs and P. Russell, “Reliability of pulse palpation by healthcare personnel to diagnose paediatric cardiac arrest,” *Resuscitation*, vol. 80, no. 1, pp. 61–64, Jan. 2009.
- [13] G. D. Perkins et al., “European Resuscitation Council Guidelines for Resuscitation 2015: Section 2. Adult basic life support and automated external defibrillation,” *Resuscitation*, vol. 95, pp. 81–99, Oct. 2015.
- [14] M. Ruppert et al., “Checking for breathing: evaluation of the diagnostic capability of emergency medical services personnel, physicians, medical students, and medical laypersons,” *Annals of Emergency Medicine*, vol. 34, no. 6, pp. 720–729, Dec. 1999.
- [15] G. D. Perkins et al., “Birmingham assessment of breathing study (BABS),” *Resuscitation*, vol. 64, no. 1, pp. 109–113, Jan. 2005.
- [16] C. Vaillancourt et al., “The impact of increased chest compression fraction on return of spontaneous circulation for out-of-hospital cardiac arrest patients not in ventricular fibrillation,” *Resuscitation*, vol. 82, no. 12, pp. 1501–1507, Dec. 2011.
- [17] A. C. H. Yu et al., “An Automated Carotid Pulse Assessment Approach Using Doppler Ultrasound,” *IEEE Transactions on Biomedical Engineering*, vol. 55, no. 3, pp. 1072–1081, Mar. 2008.
- [18] R. W. C. G. R. Wijshoff et al., “Detection of a spontaneous pulse in photoplethysmograms during automated cardiopulmonary resuscitation in a porcine model,” *Resuscitation*, vol. 84, no. 11, pp. 1625–1632, Nov. 2013.
- [19] R. W. C. G. R. Wijshoff et al., “Photoplethysmography-based algorithm for detection of cardiogenic output during cardiopulmonary resuscitation,” *IEEE Transactions on Biomedical Engineering*, vol. 62, no. 3, pp. 909–921, Mar. 2015.
- [20] T. Yagi et al., “Detection of ROSC in Patients with Cardiac Arrest During Chest Compression Using NIRS: A Pilot Study,” *Advances in Experimental Medicine and Biology*, vol. 876, pp. 151–157, 2016.
- [21] S. Parmia et al., “Cerebral Oximetry During Cardiac Arrest: A Multicenter Study of Neurologic Outcomes and Survival,” *Critical Care Medicine*, vol. 44, no. 9, pp. 1663–1674, Sep. 2016.
- [22] K. Dellimore et al., “Towards an algorithm for automatic accelerometer-based pulse presence detection during cardiopulmonary resuscitation,” in 2016 38th Annual International Conference of the IEEE Engineering in Medicine and Biology Society (EMBC), Aug. 2016, pp. 3531–3534.
- [23] L. Wei et al., “Detection of spontaneous pulse using the acceleration signals acquired from CPR feedback sensor in a porcine model of cardiac arrest,” *PLoS One*, vol. 12, no. 12, p. e0189217, 2017.
- [24] C. T. Lui, K. M. Poon, and K. L. Tsui, “Abrupt rise of end tidal carbon dioxide level was a specific but non-sensitive marker of return of spontaneous circulation in patient with out-of-hospital cardiac arrest,” *Resuscitation*, vol. 104, pp. 53–58, 2016.
- [25] P. Brinkrolf et al., “Predicting ROSC in out-of-hospital cardiac arrest using expiratory carbon dioxide concentration: Is trend-detection instead of absolute threshold values the key?” *Resuscitation*, vol. 122, pp. 19–24, 2018.
- [26] A. Elola et al., “ECG-based pulse detection during cardiac arrest using random forest classifier,” *Medical & Biological Engineering & Computing*, vol. 57, no. 2, pp. 453–462, Feb. 2019.
- [27] A. Elola et al., “Deep Neural Networks for ECG-Based Pulse Detection during Out-of-Hospital Cardiac Arrest,” *Entropy*, vol. 21, no. 3, p. 305, Mar. 2019.
- [28] A. B. Rad et al., “ECG-Based Classification of Resuscitation Cardiac Rhythms for Retrospective Data Analysis,” *IEEE Transactions on Biomedical Engineering*, vol. 64, no. 10, pp. 2411–2418, 2017.
- [29] H. Losert et al., “Thoracic-impedance changes measured via defibrillator pads can monitor signs of circulation,” *Resuscitation*, vol. 73, no. 2, pp. 221–228, May 2007.
- [30] N. Cromie et al., “Assessment of the impedance cardiogram recorded by an automated external defibrillator during clinical cardiac arrest,” *Critical Care Medicine*, vol. 38, no. 2, pp. 510–517, Feb. 2010.
- [31] E. Alonso et al., “Circulation detection using the electrocardiogram and the thoracic impedance acquired by defibrillation pads,” *Resuscitation*, vol. 99, pp. 56–62, Feb. 2016.
- [32] M. Risdal et al., “Automatic Identification of Return of Spontaneous Circulation During Cardiopulmonary Resuscitation,” *IEEE Transactions on Biomedical Engineering*, vol. 55, no. 1, pp. 60–68, Jan. 2008.
- [33] J. M. Ruiz et al., “Circulation assessment by automated external defibrillators during cardiopulmonary resuscitation,” *Resuscitation*, vol. 128, pp. 158–163, Jul. 2018.

- [34] D. P. Davis et al., "Electrical and mechanical recovery of cardiac function following out-of-hospital cardiac arrest," *Resuscitation*, vol. 84, no. 1, pp. 25–30, Jan. 2013.
- [35] A. Elola et al., "Capnography: A support tool for the detection of return of spontaneous circulation in out-of-hospital cardiac arrest," *Resuscitation*, vol. 142, pp. 153–161, 2019.
- [36] Myerburg Robert J. et al., "Pulseless Electric Activity," *Circulation*, vol. 128, no. 23, pp. 2532–2541, Dec. 2013.
- [37] L. Djordjevich et al., "Correlation Between Arterial Blood Pressure Levels and $(dZ/dt)_{min}$ in Impedance Plethysmography," *IEEE Transactions on Biomedical Engineering*, vol. 32, no. 1, pp. 69–73, Jan. 1985.
- [38] P. W. Johnston et al., "The transthoracic impedance cardiogram is a potential haemodynamic sensor for an automated external defibrillator," *European Heart Journal*, vol. 19, no. 12, pp. 1879–1888, Dec. 1998.
- [39] J. Pan and W. J. Tompkins, "A real-time QRS detection algorithm," *IEEE Transactions on Biomedical Engineering*, vol. 32, no. 3, pp. 230–236, Mar. 1985.
- [40] P. S. Hamilton and W. J. Tompkins, "Quantitative investigation of QRS detection rules using the MIT/BIH arrhythmia database," *IEEE Transactions on Biomedical Engineering*, vol. 33, no. 12, pp. 1157–1165, Dec. 1986.
- [41] I. Isasi et al., "A Machine Learning Shock Decision Algorithm for Use During Piston-Driven Chest Compressions," *IEEE Transactions on Biomedical Engineering*, vol. 66, no. 6, pp. 1752–1760, Jun. 2019.
- [42] I. Isasi et al., "Automatic Cardiac Rhythm Classification With Concurrent Manual Chest Compressions," *IEEE Access*, vol. 7, pp. 115 147–115 159, 2019.
- [43] J. Ruiz et al., "Reliable extraction of the circulation component in the thoracic impedance measured by defibrillation pads," *Resuscitation*, vol. 84, no. 10, pp. 1345–1352, Oct. 2013.
- [44] S. Ruiz de Gauna et al., "A method to remove CPR artefacts from human ECG using only the recorded ECG," *Resuscitation*, vol. 76, no. 2, pp. 271–278, Feb. 2008.
- [45] J. Ruiz et al., "Cardiopulmonary resuscitation artefact suppression using a Kalman filter and the frequency of chest compressions as the reference signal," *Resuscitation*, vol. 81, no. 9, pp. 1087–1094, Sep. 2010.
- [46] O. El B'charri et al., "ECG signal performance de-noising assessment based on threshold tuning of dual-tree wavelet transform," *Biomedical Engineering Online*, vol. 16, no. 1, p. 26, Feb. 2017.
- [47] H. Kwok et al., "Electrocardiogram-based pulse prediction during cardiopulmonary resuscitation," *Resuscitation*, vol. 147, pp. 104–111, Feb. 2020.
- [48] W. Chen et al., "Characterization of surface EMG signal based on fuzzy entropy," *IEEE Transactions on Neural Systems and Rehabilitation Engineering*, vol. 15, no. 2, pp. 266–272, Jun. 2007.
- [49] W. Chen et al., "Measuring complexity using FuzzyEn, ApEn, and SampEn," *Medical Engineering & Physics*, vol. 31, no. 1, pp. 61–68, Jan. 2009.
- [50] B. Chicote et al., "Application of Entropy-Based Features to Predict Defibrillation Outcome in Cardiac Arrest," *Entropy*, vol. 18, no. 9, p. 313, Sep. 2016.
- [51] C. Figuera et al., "Machine Learning Techniques for the Detection of Shockable Rhythms in Automated External Defibrillators," *PloS One*, vol. 11, no. 7, p. e0159654, 2016.
- [52] G. Ristagno et al., "Amplitude spectrum area to guide resuscitation—a retrospective analysis during out-of-hospital cardiopulmonary resuscitation in 609 patients with ventricular fibrillation cardiac arrest," *Resuscitation*, vol. 84, no. 12, pp. 1697–1703, Dec. 2013.
- [53] I. Jekova and V. Krasteva, "Real time detection of ventricular fibrillation and tachycardia," *Physiological Measurement*, vol. 25, no. 5, pp. 1167–1178, Oct. 2004.
- [54] T. Hastie, R. Tibshirani, and J. Friedman, *The Elements of Statistical Learning: Data Mining, Inference, and Prediction*, Second Edition. Springer, May 2017.
- [55] P. Pudil et al., "Floating search methods for feature selection with non-monotonic criterion functions," in *Proceedings of the 12th IAPR International Conference on Pattern Recognition*, Oct. 1994, pp. 279–283.
- [56] P. Pudil, J. Novovičová, and S. Bláha, "Statistical approach to pattern recognition: Theory and practical solution by means of PREDITAS system," *Kybernetika*, vol. 27, no. Suppl, pp. (1)–76, 1991.
- [57] S. D. Stearns, "On Selecting Features for Pattern Classifiers," in *Third Int. Conf. on Pattern recognition*, Coronada, CA, 1976, pp. 71–75.
- [58] B. E. Boser, I. M. Guyon, and V. N. Vapnik, "A training algorithm for optimal margin classifiers," in *Proceedings of the fifth annual workshop on Computational learning theory*, ser. COLT '92, Jul. 1992, pp. 144–152.
- [59] C. Cortes and V. Vapnik, "Support-vector networks," *Machine Learning*, vol. 20, no. 3, pp. 273–297, Sep. 1995.
- [60] G. James et al., *An Introduction to Statistical Learning: with Applications in R*, 7th ed. New York: Springer, Jun. 2013.
- [61] C. C. Chang and C. J. Lin, "LIBSVM: A library for support vector machines," *ACM Transactions on Intelligent Systems and Technology*, vol. 2, Jul. 2007.
- [62] D. Snyder and C. Morgan, "Wide variation in cardiopulmonary resuscitation interruption intervals among commercially available automated external defibrillators may affect survival despite high defibrillation efficacy," *Critical Care Medicine*, vol. 32, no. 9 Suppl, pp. S421–424, Sep. 2004.



ERIK ALONSO was born in Basauri, Spain, in 1987. He received the BEng, MSc and PhD degrees from the University of the Basque Country (UPV/EHU) in 2010, 2011 and 2014, respectively. He is currently an associate professor with the Department of Applied Mathematics at the University of the Basque Country (UPV/EHU). His research interests include biomedical signal processing, data management and machine learning applied to data from prehospital emergency care and cardiac arrest. In this field, he has collaborated with leading international clinicians and researchers, and he has published over 20 papers in SCI-IF journals, and contributed over 50 communications in scientific conferences.



UNAI IRUSTA was born in Bilbao, Spain, in 1973. He received the M.Sc. Degree in Telecommunications engineering with honors in 1998 from the University of the Basque Country (UPV/EHU). After working for international companies in the Mobile Communications sector, he joined UPV/EHU as assistant professor in 2003, and as associate professor since 2011. He is founding member of the Bioengineering and Resuscitation research group, recognized as outstanding in the Basque Science System. His field of expertise are biomedical signal processing, machine learning, and data management in the field of pre-hospital emergency medicine and cardiac arrest. In this field, he has collaborated with leading European and US clinicians, and he has published over 40 papers in SCI-IF journals, and contributed over 100 communications in scientific conferences.



ELISABETE ARAMENDI was born in Azkoitia, Spain, in 1969. She received the M.Sc. Degree in Telecommunications engineering in 1993 from the University of the Basque Country (UPV/EHU), where she has been an assistant professor since 1994 and associate professor since 2002. She is founding member and director of the Bioengineering and Resuscitation research group, recognized as outstanding in the Basque Science System. Her field of expertise are statistical signal processing, biomedical signal processing and data management in the field of pre-hospital emergency medicine and cardiac arrest. In this field, she has collaborated with leading researchers of the Regional Outcomes Consortium (ROC), and she has published over 40 papers in SCI-IF journals, and contributed over 100 communications in scientific conferences.



MOHAMUD R. DAYA was born in Nairobi, Kenya. He received his BSc and MD degrees from the University of British Columbia in 1980 and 1984. In 1998, he received a MSc degree from the London School of Hygiene & Tropical Medicine. He is currently a professor of Emergency Medicine at the Oregon Health & Science University in Portland, Oregon, USA. His research interests include the management of time critical emergencies including cardiac arrest, acute coronary syndrome, acute stroke and life-threatening trauma in the out-of-hospital setting. He has collaborated extensively with biomedical engineers on topics related to signal processing and has published more than 130 peer reviewed manuscripts.

• • •